Ultraviolet Photodepletion Spectroscopy of Dibenzo-18-Crown-6-Ether Complexes with Alkali Metal Cations

Chang Min Choi, Hwan Jin Kim, Jun Ho Lee, Won Jik Shin, Tae Oh Yoon,† and Nam Joon Kim*

Department of Chemistry, Chungbuk National University, Chungbuk 361-763, Korea

Jiyoung Heo*

Division of Chemistry and Chemical Engineering, California Institute of Technology, Pasadena, California

Received: April 26, 2009; Revised Manuscript Received: June 5, 2009

Ultraviolet photodepletion spectra of dibenzo-18-crown-6-ether complexes with alkali metal cations (M^+-DB18C6, M = Cs, Rb, K, Na, and Li) were obtained in the gas phase using electrospray ionization quadrupole ion-trap reflectron time-of-flight mass spectrometry. The spectra exhibited a few distinct absorption bands in the wavenumber region of 35 450−37 800 cm^{-1}. The lowest-energy band was tentatively assigned to be the origin of the S_0-S_1 transition, and the second band to a vibronic transition arising from the "benzene breathing" mode in conjunction with symmetric or asymmetric stretching vibration of the bonds between the metal cation and the oxygen atoms in DB18C6. The red shifts of the origin bands were observed in the spectra as the size of the metal cation in M^+-DB18C6 increased from Li^+ to Cs^+. We suggested that these red shifts arose mainly from the decrease in the binding energies of larger-sized metal cations to DB18C6 at the electronic ground state. These size effects of the metal cations on the geometric and electronic structures, and the binding properties of the complexes at the S_0 and S_1 states were further elucidated by theoretical calculations using density functional and time-dependent density functional theories.

Introduction

Since the first discovery by Pedersen in 1967,[1,2] crown ethers have drawn much attention due to their ability to selectively bind various cations in solution.[3,4] With this unique property, the potential applications of crown ethers have been found in many diverse and practical areas. For example, crown ethers have been proposed as separating agents to sequester high-level nuclear wastes,[5] as ligating agents to transport ions through membranes,[6] as phase transfer catalysts,[7] or as probes to reveal equilibrium structures and folding states of proteins.[8] In addition, crown ethers have been a model system to study the specificity of enzymes, molecular recognition processes in host−guest chemistry and noncovalent interactions of multidentate ligands.[4]

One of the most intriguing subjects for crown ethers has been therefore to elucidate the origin of their selectivity for metal cations. It has long been believed that the selectivity stems from the size relationship between the metal cation and the cavity of crown ether; the strongest binding affinity of 18-crown-6-ether (18C6) to a potassium ion (K^+) of all alkali metal cations was explained by this size relationship.[3,4] However, it was found later that the order of the binding affinity in the gas phase is quite different from that in solution.[9−12] In the gas phase the binding affinity is the strongest for Li^+ and decreases as the radius of the metal cation becomes larger, while that in solution is in the order of $K^+ > Rb^+ > Cs^+ > Na^+ > Li^+$,[3] manifesting the role of solvation in the selectivity. Therefore, they concluded that the selectivity of crown ethers in solution is determined not by the size-relationship but by the interplay between the solvation energies of metal cations and their intrinsic binding energies to crown ethers.[13−15] This clearly demonstrates the importance of studies on crown ethers in the isolated gas phase, where there is no solvent or other species around them that could dissemble the intrinsic properties of crown ethers through incessant interactions with them.

The advent of the electrospray ionization (ESI) method combined with mass spectrometry[16] provides a powerful tool to study nonvolatile and large-sized molecules in the gas phase. This technique has also been extensively employed in studies on crown-ether complexes with metal cations. The gas-phase selectivity of crown ethers was investigated by measuring relative abundances of the product ions generated by high-energy dissociation of the crown-ether complexes with two different alkali-metal cations.[11] Intrinsic binding affinities and complexation rates for alkali-metal cations were determined from the ion−molecule reaction of crown ethers in the gas phase.[9] Bond-dissociation energies of gas-phase crown-ether complexes with alkali-metal cations were measured from the thresholds of collision-induced dissociation.[12] Recently, Ebata and co-workers[17] reported the laser-induced fluorescence spectra of benzo-18-crown-6 (B18C6), dibenzo-18-crown-6 (DB18C6), and their hydrated complexes produced in a supersonic jet.

However, there has been no spectroscopic studies on crown-ether complex ions performed in the gas phase as far as we know, which have critical importance in understanding the photophysical and -chemical properties that are necessary for development of crown-ether based fluoroionophores[18,19] or supramolecular photonic devices.[20,21]

Only a few studies on the properties of crown-ether complex ions in an excited state have been carried out in the solution

* To whom correspondence should be addressed. E-mail: (N.J.K.) namjkim@chungbuk.ac.kr; (J.H.) jiyoung.heo@gmail.com.
† Present address: Korea Research Institute of Standards and Science, Daejon, Korea.

10.1021/jp903832w CCC: $40.75
Published on Web 07/01/2009

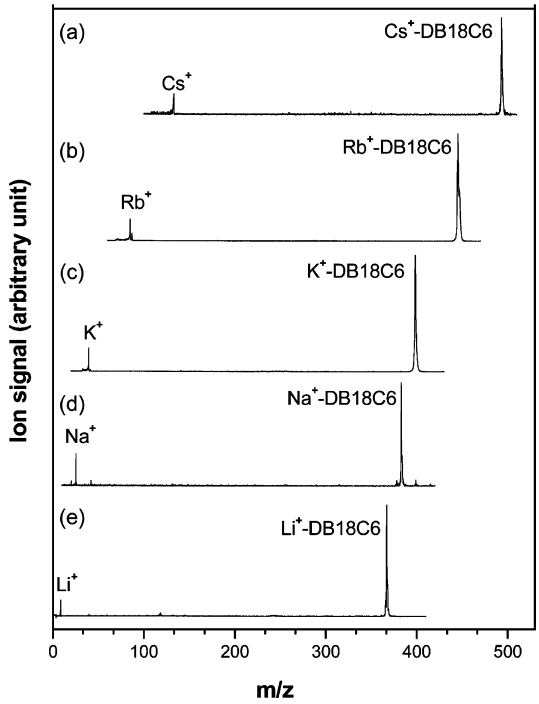

Figure 1. Mass spectra of M^+-DB18C6 (M = Cs, Rb, K, Na, and Li).

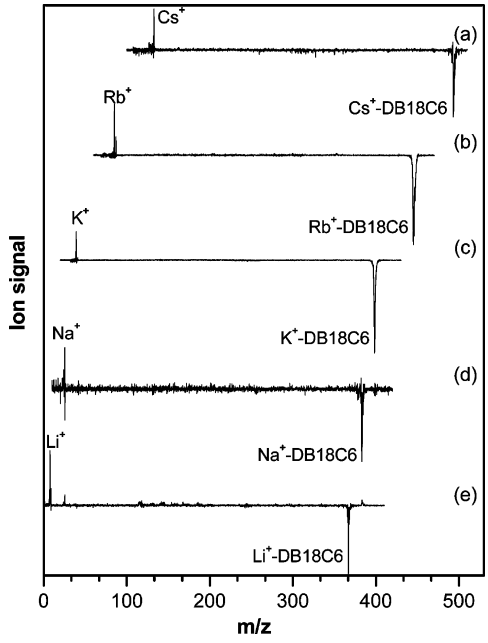

Figure 2. Difference mass spectra of M^+-DB18C6 obtained by subtracting the ion signals without laser pulses from those with laser pulses irradiated onto the ions in the QIT.

phase. It was reported that the excited-state properties of crown ethers were drastically altered by binding of metal cations.[22] The enhancement of fluorescence quantum yield was observed for DB18C6 upon complexation with alkali metal cations in methanol.[23] The stronger fluorescence in the presence of alkali metal cations was also reported in pyrene- and anthracene-appended crown ether derivatives.[19] Nakamura et al.[24] showed that the stability constants of crowned spirobenzopyran derivatives with metal cations decreased dramatically in methanol by visible irradiation. The selective complexation of metal cations by DB18C6 bridging porphyrin-fullerene dyad was found to facilitate the electron transfer or energy transfer from the

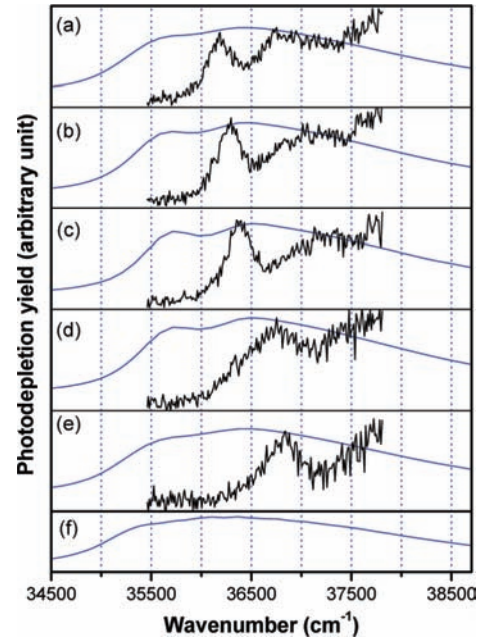

Figure 3. UV photodepletion spectra of (a) Cs^+-, (b) Rb^+-, (c) K^+-, (d) Na^+-, and (e) Li^+-DB18C6 in the gas phase. (f) UV absorption spectrum of DB18C6 in methanol. The gas-phase spectra are overlapped with the corresponding absorption spectra of M^+-DB18C6 in methanol.

photoexcited porphyrin to fullerene by changing the bridge conformation and electronic orbital distribution influencing electronic coupling.[21]

In this paper, as a first step to understand the intrinsic photophysical and -chemical properties of crown ethers, UV photodepletion spectra of DB18C6 complexes with alkali metal cations (M^+-DB18C6) were obtained in the gas phase using ESI and quadrupole ion-trap reflectron time-of-flight mass spectrometry (QIT-reTOF). DB18C6 was chosen because it contains benzene rings as chromophores for an UV radiation. Moreover, with the proximity of benzene rings to the cavity of DB18C6 UV absorption spectra could be used in monitoring the interactions between DB18C6 and the metal cations.

The photodepletion spectra of M^+-DB18C6 exhibited a few distinct absorption bands in their lowest-energy absorption region. The red shifts of the origin bands of the S_0-S_1 transition were observed as the size of a metal cation in M^+-DB18C6 increased from Li^+ to Cs^+. The reason for this size effect, which turned out to be closely related with the binding energy of the metal cation to DB18C6, was elucidated by theoretical calculations using density functional (DFT) and time-dependent density functional theories (TD-DFT).

Experimental Section

The experimental apparatus is a quadrupole ion-trap reflectron time-of-flight mass spectrometer (QIT-reTOFMS). The details of the experimental setup were described elsewhere[25] and only a brief description is given here.

DB18C6, LiCl, NaCl, KCl, RbCl, and CsCl were all purchased from Sigma-Aldrich and used without further purification. Each powder sample was dissolved in methanol at a concentration of 200 μM, and the DB18C6 solution was mixed with each alkali metal solution to produce DB18C6 complexed with an alkali metal cation. Then, the mixed solutions were electrosprayed into ion droplets through a nozzle floated to +3.5

TABLE 1: The Energies and Widths of the Peaks Observed in the Photodepletion Spectra of M^+-DB18C6 (in cm^{-1})

	lowest-energy peak			second lowest-energy peak		
	energy	width	relative energy	energy	width	gap[a]
Cs^+-DB18C6	36173 ± 12	240 ± 10	−612	36780 ± 17	490 ± 30	607
Rb^+-DB18C6	36268 ± 10	250 ± 10	−517	36910 ± 27	570 ± 80	642
K^+-DB18C6	36375 ± 7	240 ± 10	−410	37083 ± 35	460 ± 50	708
Na^+-DB18C6	36674 ± 37	620 ± 30	−111			
Li^+-DB18C6	36785 ± 12	350 ± 30	0			

[a] The differences in energies between the lowest- and the second lowest-energy peak.

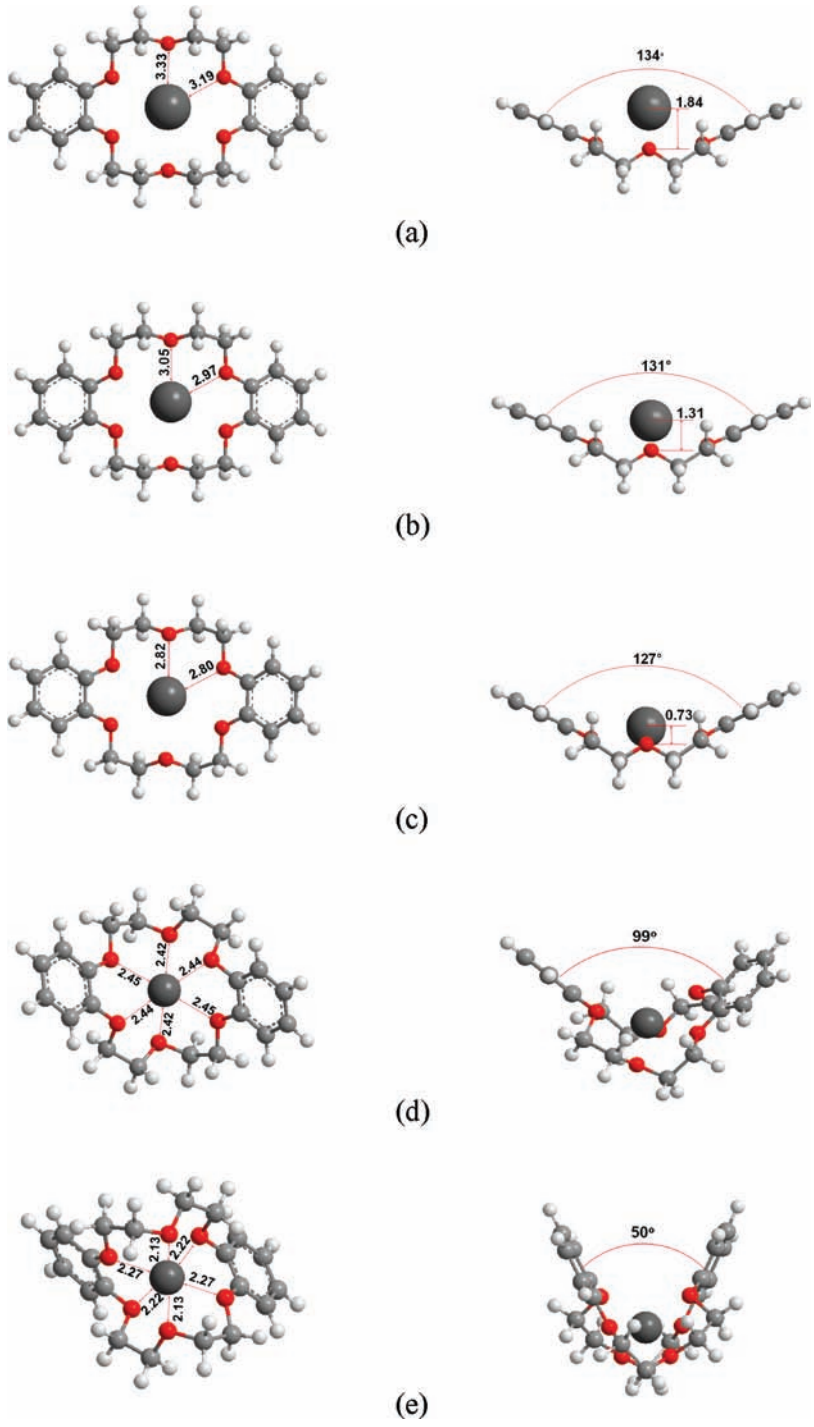

Figure 4. The most stable geometries of (a) Cs^+-, (b) Rb^+-, (c) K^+-, (d) Na^+-, and (e) Li^+-DB18C6 optimized at the B3LYP/6-31+G* level. The top views are on the left and the side views on the right.

kV. The ion droplets were desolvated while passing through a heated capillary and entered into a QIT through a skimmer.

Each of two end-caps of QIT has a hole of 3 mm diameter for ion beams, and the ring electrode has two holes of 2.2 mm

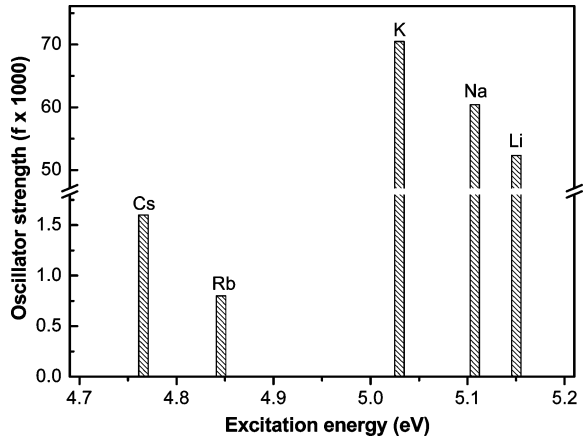

Figure 5. Plot of the excitation energies to the S_1 state of M^+-DB18C6 (M = Cs, Rb, K, Na, and Li) predicted by TD-DFT at the B3LYP/6-31+G* level.

diameter for laser beams. For ion storage, a radio frequency (rf) signal of a constant frequency (1 MHz) and amplitude (+2.5 kV) was applied to the ring electrode with both end-caps grounded. A coldfinger from a liquid nitrogen reservoir was attached to the QIT for cooling the ions. The temperature of QIT was measured to be at around 150 K.

After 48 ms of ion accumulation, the broadband stored waveform inverse Fourier transform (SWIFT)[26] pulses were applied to the exit end-cap of QIT for isolation of M^+-DB18C6 from other residual ions. The SWIFT was generated by an arbitrary function generator (AFG 3022, Tektronix) using the algorithm developed by Doroshenko and Cotter.[27]

After application of the SWIFT for 40 ms, the frequency-doubled output of a dye laser pumped by the third harmonic of an Nd:YAG laser was irradiated into the QIT for photodissociation of the isolated ions. Then, a positive DC pulse was applied to the entrance end-cap to extract all of the ions in the QIT out to a reflectron TOF-MS for mass analysis. The ions were reflected by a reflectron and detected with a 40 mm dual microchannel plate (MCP). The ion signals from the MCP were processed by a digital storage oscilloscope.

The timings of the ion storage, extraction and detection were synchronized by TTL pulses from a digital delay generator.

The photodepletion spectra were obtained by recording photodepletion yields (I_{pd}) as a function of the laser wavelength. The photodepletion yield was determined by

$$I_{pd} = \frac{I_{off} - I_{on}}{I_{off}} \quad (1)$$

where I_{on} and I_{off} are the ion intensities of M^+-DB18C6 measured with and without irradiation of laser pulses, respectively. From the measurement of the power dependence of the laser pulse, the photodepletion of M^+-DB18C6 was found to be a single-photon process. We observed a slope of ~1.0 in the plot of $\log(I_{pd})$ versus log(laser power). The photodepletion spectra were calibrated against the variation of laser fluence over the frequency.

Computational Methods

The conformational searches were performed to find initial conformers of M^+-DB18C6 within the energy of 20 kJ/mol using a Metropolis Monte Carlo method with the AMBER* force field in the Macromodel package (Schrödinger, LLC: New York). The geometries of the initial conformers were fully optimized by a series of theoretical calculations at the HF/3-21G, HF/6-31G, and then B3LYP/6-31G levels. Then, the conformers within 2 kcal/mol were further optimized at the B3LYP/6-31+G(d) level. In all of those calculations, we used the Los Alamos effective-core potential LANL2DZ as a basis set for alkali metals and referred to this basis set as 6-31+G* in the remainder of this paper. The vibrational analyses at the same level of theory were performed to find no imaginary vibrational frequencies for all of the lowest-energy structures. The singlet excitation energies were calculated using TD-DFT at the B3LYP/6-31+G* level.

All calculations were carried out using the GAUSSIAN 03 package.[28]

Results

Figure 1 shows the mass spectra of M^+-DB18C6 (M = Cs, Rb, K, Na, and Li) obtained using QIT-reTOFMS with SWIFT pulses applied to the QIT. In the mass spectra, the ion signals of M^+-DB18C6 were observed with those of the corresponding alkali metal cations that were generated from metastable dissociation of M^+-DB18C6 in the QIT.

Figure 2 shows the difference mass spectra obtained by subtracting the ion signals without laser pulses from those with laser pulses irradiated onto the ions in the QIT. The negative signals, therefore, represent the depleted-ion intensities and the positive ones the fragment-ion intensities generated from the subsequent photoinduced dissociation (PID). Apart from the alkali metal cations, no other photofragment ions were detected. This was also true with the laser pulses at other wavelengths that M^+-DB18C6 could absorb. Therefore, we concluded that the PID of M^+-DB18C6 produced only M^+ as fragment ions.

Figure 3 shows the photodepletion spectra of M^+-DB18C6 in the wavenumber range of 35 450−37 800 cm^{-1} (282−265 nm) overlapped with the UV absorption spectra of the corresponding M^+-DB18C6 in methanol. We assumed that the excitation-energy dependence of the photodepletion yields resulted mainly from the energy dependence of molecular absorption coefficients.[29,30] Since no other peaks were observed below 35 450 cm^{-1}, we tentatively assigned the lowest-energy peak in each photodepletion spectrum as the origin band of the S_0-S_1 transition. The energies and widths of the peaks in the spectra were measured by fitting the spectra to Gaussian functions and listed in Table 1. The origin bands exhibited the red shifts as the size of the metal cation bound to DB18C6 increased, which was a little ambiguous, though, in the UV absorption spectra taken in solution, manifesting the importance of the gas-phase studies over the solution-phase ones.

It was also found that the origin bands in the photodepletion spectra were all blue shifted from the lowest-energy bands in the corresponding UV absorption spectra. These blue shifts are typical because in most cases the solvation stabilizes the electronic excited state more than the ground state. It is noteworthy, however, that the amounts of the blue shift for Li^+- and Na^+-DB18C6 are about two times larger than those for the other M^+-DB18C6. This indicates much larger stabilization of the excited states for Li^+- and Na^+-DB18C6 by solvation, which might indicate the significant structural difference from the other DB18C6 in complex with a larger metal cation. This turns out to be true in the following geometry optimization for M^+-DB18C6.

Figure 4 shows the optimized geometries of M^+-DB18C6 at the B3LYP/6-31+G* level of theory. Different from the boat-

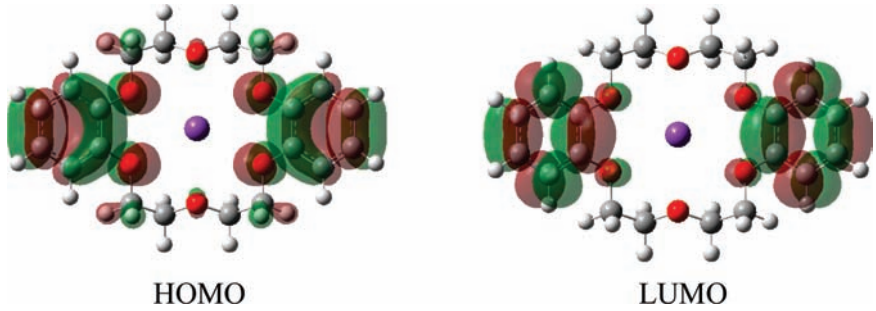

Figure 6. Pictorial representations of HOMO and LUMO of K^+-DB18C6.

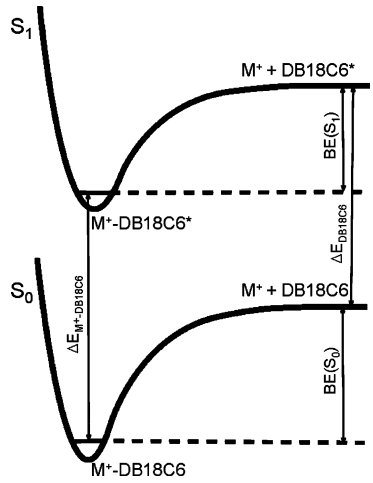

Figure 7. Schematic diagram of the potential energy curves of M^+-DB18C6 illustrating the symbols used in the eq 2.

TABLE 2: The Binding Energies of Alkali Metal Cations to DB18C6 at the S_0 and S_1 States (in eV)

	S_1[a]	$BE(S_0)$[b]	$BE(S_1)$[c]	relative ratio[d]	difference[e]
Cs^+-DB18C6	4.48	1.41	1.34	95.0%	0.07
Rb^+-DB18C6	4.50	1.60	1.51	94.4%	0.09
K^+-DB18C6	4.51	2.29	2.19	95.6%	0.10
Na^+-DB18C6	4.55	3.10	2.96	95.5%	0.14
Li^+-DB18C6	4.56				
DB18C6	4.41[f]				

[a] Experimental excitation energies to the origin band of the S_0-S_1 transition. [b] Experimental binding energies of the metal cations to DB18C6 at the S_0 state (ref 10). [c] Binding energies of the metal cations to DB18C6 at the S_1 state estimated in this study. [d] Percent ratios of the binding energy at the S_1 state relative to that at the S_0 state. [e] Differences in the binding energies between the S_0 and S_1 states in eV. [f] Reference 17.

shaped structures with C_{2v} symmetry as the most stable structures of K^+-, Rb^+- and Cs^+-DB18C6, those of Li^+- and Na^+-DB18C6 were predicted to be slightly twisted structures; the global minimum structure of DB18C6 was predicted to be the boat-shaped one.[17] The twisted structures were also reported as the most stable ones for Li^+- and Na^+-DB18C6 by Dearden and co-workers.[10] However, their structures are different from ours. In our prediction, the most stable structures of Li^+- and Na^+-DB18C6 have two benzene rings facing each other at the angles of 50 and 99°, respectively, indicating the contribution of the stacking interaction between two benzene rings in stabilizing the structures, while those predicted by them have the angles of near 180°. This discrepancy seems to result from the difference in the theoretical methods used to find the most stable structures; they employed the HF/LANL2DZ level of theory instead of our B3LYP/6-31+G*. However, it was further confirmed from the single point energy calculations using the second-order Møller−Plesset perturbation theory with the 6-31+G* basis set that our structures were more stable than theirs.

The reason for adopting the twisted geometries for Li^+- and Na^+-DB18C6 is smaller radii of Li^+ and Na^+ than that of the cavity in DB18C6.[31−33] With the smaller radii of Li^+ and Na^+, both metal cations draw the six oxygen atoms around the cavity toward them, which makes the distances between the metal cation and the oxygen atoms shorter than those in the boat-shaped one, and the resulting steric effects among oxygen atoms lead to the twisted geometry. For instance, the average distance from the oxygen atoms to Na^+ is 2.44 Å in the twisted structure, while that is 2.64 Å in the local-minimum boat-shaped one. This implies that the electrostatic interactions between the metal cation and the oxygen atoms indeed play dominant roles in binding of the metal cation, as was reported previously.[15]

With a near coincidence of the radius of K^+ (1.38 Å) to the cavity radius (1.34−1.43 Å), K^+ is located at the center of the cavity in the lowest-energy structure, where DB18C6 has a symmetric boat-shaped structure. In the Rb^+- and Cs^+-DB18C6, with larger radii of Rb^+ and Cs^+ than the cavity, they are placed slightly above the center of cavity in the boat-shaped structure. The average distance from the six oxygen atoms to the metal cation gets longer from 2.81 Å for K^+-DB18C6 to 3.24 Å for Cs^+-DB18C6. In addition, the angle between the two benzene rings increases from 127 to 134° with the radius of the metal cation increasing from K^+ to Cs^+.

The excitation energies to the S_1 state of M^+-DB18C6 were calculated by TD-DFT at the optimized geometries and plotted in Figure 5. The red shifts of the origin bands from Li^+- to Cs^+-DB18C6 observed in the photodepletion spectra were reproduced well in the calculations. The weaker oscillator strengths of Cs^+- and Rb^+-DB18C6 than those of other M^+-DB18C6 in the plot, however, are likely to result from the failure of TD-DFT in estimating the oscillator strengths correctly, because the absorption intensities of the origin bands for Cs^+- and Rb^+-DB18C6 are observed to be comparable with those of other complex ions. Even though TD-DFT is quite reliable for predicting the excitation energies to low-lying electronic states, it was reported that the corresponding oscillator strengths might be less accurate and even erroneous, especially for open-shell or charged systems.[34−36] The pictorial representations for highest occupied molecular orbital (HOMO) and lowest unoccupied molecular orbital (LUMO) of K^+-DB18C6 are also shown in Figure 6. Those for the other complex ions are in the Supporting Information. It was predicted that the excitation to the S_1 state of M^+-DB18C6 arose mainly from the $\pi-\pi^*$ transition of benzene moieties.

TABLE 3: The Contribution of 2p Orbitals of the Six Oxygen Atoms in M^+-DB18C6 to the Density of Electron in HOMO and LUMO

	Li^+-DB18C6	Na^+-DB18C6	K^+-DB18C6	Rb^+-DB18C6	Cs^+-DB18C6
HOMO	6.37×10^{-2}	6.41×10^{-2}	1.17×10^{-1}	1.36×10^{-1}	1.24×10^{-1}
LUMO	3.81×10^{-5}	2.35×10^{-4}	4.24×10^{-4}	6.00×10^{-4}	5.33×10^{-4}
reduction ratio (LUMO/HOMO)	5.98×10^{-4}	3.67×10^{-3}	3.62×10^{-3}	4.41×10^{-3}	4.30×10^{-3}

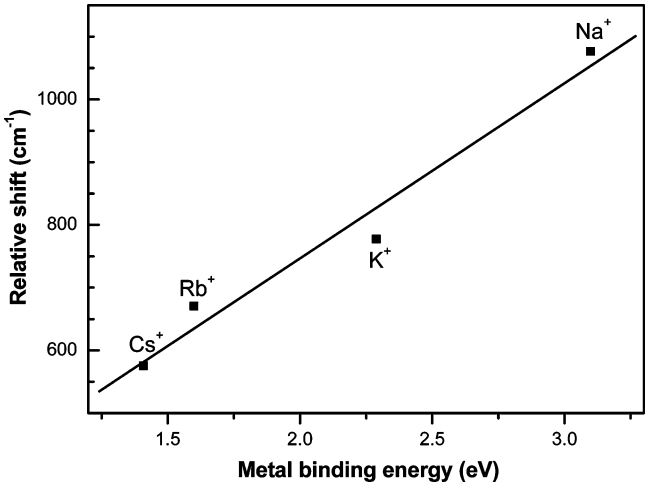

Figure 8. Plot of the relative shift, $\Delta E_{M^+-DB18C6} - \Delta E_{DB18C6}$, versus the binding energy of the metal cation to DB18C6 at the electronic ground state. $\Delta E_{M^+-DB18C6}$ and ΔE_{DB18C6} are the excitation energies to the origin bands of the S_0-S_1 transition of M^+-DB18C6 and DB18C6, respectively.

Discussion

The most interesting feature in the photodepletion spectra of M^+-DB18C6 is that the origin band is red shifted as the radius of the metal cation increases from Li^+ to Cs^+.

Noting that the most red-shifted origin band of Cs^+-DB18C6 is still bluer than that of bare DB18C6,[17] we can conclude that the electronic ground state of DB18C6 is more stabilized than its electronic excited state upon binding any alkali metal cation and that the difference in the stabilization energies between the ground and excited states determines the amount of the blue shift. The largest blue shift from the origin of DB18C6 is thus observed for Li^+-DB18C6 and the least for Cs^+-DB18C6; this appears as the red shifts of origin bands from Li^+- to Cs^+-DB18C6 in the photodepletion spectra. The stabilization energy is equal to the binding energy of the metal cation to DB18C6. Therefore, we conclude that the difference in the binding energies between the ground and the excited state is the largest for Li^+-DB18C6 and the smallest for Cs^+-DB18C6.

The binding energies at the ground state were reported to decrease as the radius of the metal cation increased from Li^+ to Cs^+.[10,12] The binding energies at the excited state could be estimated by

$$\mathrm{BE}(S_1) = \mathrm{BE}(S_0) + \Delta E_{DB18C6} - \Delta E_{M^+-DB18C6} \quad (2)$$

where $\mathrm{BE}(S_1)$ and $\mathrm{BE}(S_0)$ are the binding energies of the metal cation at the S_1 and S_0 states, respectively, and ΔE_{DB18C6} and $\Delta E_{M^+-DB18C6}$ are the excitation energies to the origin bands of DB18C6 and M^+-DB18C6, respectively (Figure 7). The $\mathrm{BE}(S_1)$'s for M^+-DB18C6 were listed in Table 2; the value for Li^+-DB18C6 was absent because the experimental binding energy of Li^+ at the S_0 was not available.

The $\mathrm{BE}(S_1)$'s amount to 94.4−95.6% of the corresponding $\mathrm{BE}(S_0)$'s. These smaller binding energies at the excited state can be explained by the reduction in the contribution of the atomic orbitals of four oxygen atoms near the benzene moieties to the density of electron in a given molecular orbital (MO) upon excitation from HOMO to LUMO (Figure 6). Metal cations are bound in the cavity of DB18C6 via interactions with six oxygen atoms acting as electron donors. In particular, the four of them near the benzene moieties have larger contribution to the electron density of HOMO and will play more dominant roles in binding to the metal cation than the other oxygen atoms. Therefore, the decrease in their contribution to the electron density of LUMO may lead to the weaker binding at the S_1 state.

Moreover, the relative ratios of the binding energies for the S_1 to the S_0 state are nearly the same for all M^+-DB18C6. This can be also understood from the variation in the contribution of 2p orbitals of the six oxygen atoms to the electron density of an overall MO from HOMO to LUMO. The electrons in 2p orbitals of the oxygen atoms, especially the nonbonding electrons, are expected to play major roles as electron donors in the electrostatic interactions with the metal cation in M^+-DB18C6. It was predicted that the contribution of the 2p orbitals, which was calculated from the squares of MO coefficients for the $2p_x$, $2p_y$ and $2p_z$ orbitals of six oxygen atoms in M^+-DB18C6 divided by the sum of those for all atomic orbitals in the MO,[37] was reduced by almost the same amount for all M^+-DB18C6 upon excitation from HOMO to LUMO (Table 3).

It is also found that the difference between the $\mathrm{BE}(S_1)$ and $\mathrm{BE}(S_0)$ decreases with the size of the metal cation increasing from Na^+ to Cs^+, resulting in the red shifts of origin bands from Na^+- to Cs^+-DB18C6. Considering that the relative ratios of the $\mathrm{BE}(S_1)$ to $\mathrm{BE}(S_0)$ are about the same for all M^+-DB18C6, which may imply that the characteristics of the binding in the S_1 state is largely determined by that in the S_0 state, we suggest that the smaller difference between the $\mathrm{BE}(S_1)$ and $\mathrm{BE}(S_0)$ for a larger metal cation is due to its smaller binding energy to DB18C6 at the S_0.

This can be speculated as follows. The difference in the excitation energies to the origin bands between M^+-DB18C6 and DB18C6 can be formulated from the eq 2 by

$$\Delta E_{M^+-DB18C6} - \Delta E_{DB18C6} = \mathrm{BE}(S_0) - \mathrm{BE}(S_1) = \mathrm{BE}(S_0) \times (1 - R) \quad (3)$$

where R is the reduction ratio of the binding energy upon excitation from the S_0 to the S_1 state. With almost the same values of R for all M^+-DB18C6, the difference in the energies of the origin bands is determined by $\mathrm{BE}(S_0)$. The reliability of the above equation is tested by the linearity of the plot in Figure 8, where the difference, $\Delta E_{M^+-DB18C6} - \Delta E_{DB18C6}$, is plotted against the binding energy of the metal cation at the S_0.

Another interesting feature observed in Figure 3 is that the widths of origin bands of Li^+- and Na^+-DB18C6 are about 1.4 and 2.6 times broader, respectively, than those of K^+-, Rb^+-,

and Cs^+-DB18C6. This spectral broadening may be caused by lifetime broadening or thermal broadening or conformational inhomogeneity. As for the lifetime broadening, the broader band widths may arise from a shorter excited-state lifetime of Li^+- or Na^+-DB18C6 than those of the other M^+-DB18C6. However, this is the least plausible because the fluorescence lifetimes of M^+-DB18C6 measured in methanol were all in the range of 2.8−3.8 ns.[23]

The possibility of thermal broadening as the cause for broader origin bands of Li^+- and Na^+-DB18C6 is also rather low due to the following reasons: First, all M^+-DB18C6 have nearly the same internal temperatures under our experimental conditions. Second, all M^+-DB18C6 have almost the same low-frequency vibrational modes at similar energies, which may be excited with the thermal energy at 150 K and contribute to the spectral broadening as hot bands.

Therefore, we suggest that the conformational inhomogeneity is more likely to cause the broader origin bands for Li^+- and Na^+-DB18C6. This is supported by the number of possible conformers found by the AMBER* conformational search within the energy of 20 kJ/mol. The numbers for Li^+- and Na^+-DB18C6 are 64 and 64, while those for K^+-, Rb^+-, and Cs^+-DB18C6 are 5, 8, and 5, respectively. Following the sequential geometric optimizations at the HF/3-21G, HF/6-31G, B3LYP/6-31G, and B3LYP/6-31+G* levels, the numbers of conformers within 2 kcal/mol reduce to 4, 4, 1, 2, and 2 for Li^+-, Na^+-, K^+-, Rb^+-, and Cs^+-DB18C6, respectively. Thus, the superposition of the origin bands from a little larger number of different conformers could result in the broader band widths for Li^+- and Na^+-DB18C6 than those for the other M^+-DB18C6.

The second lowest-energy bands, which were clearly shown in the spectra of K^+-, Rb^+- and Cs^+-DB18C6, were tentatively assigned to be a vibronic band arising from a combination of vibrations, the "benzene breathing" vibration and the symmetric or asymmetric stretching vibration of bonds between the metal cation and the four oxygen atoms neighboring the benzene moieties. We assumed that the second bands in the three complex ions result from the same vibrational mode, because of the similarities in their geometric and electronic structures, and also in the spectral aspects observed in the solution and gas-phase spectra (Figure 3).

The assignment was done by considering the following: First, the energy differences between the origin and the second lowest-energy band are 708, 642, and 607 cm^{-1} for K^+-, Rb^+-, and Cs^+-DB18C6, respectively. Second, since the main feature of the S_1 state of M^+-DB18C6 arises from the benzene rings and the neighboring four oxygen atoms (Figure 6), the vibrational modes coupled to the electronic transition are likely to be mainly constituted by benzene-ring vibrations, along with additional vibrations involving the four oxygen atoms.

Conclusion

UV photodepletion spectra of M^+-DB18C6 (M = Cs, Rb, K, Na, and Li) were obtained in the gas phase using electrospray ionization and quadrupole ion trap reflectron time-of-flight mass spectrometry. The red shifts of the origin bands were observed as the radius of the metal cation in the complex ion increased from Li^+ to Cs^+. We suggested that the red shifts arise mainly from the differences in the binding energies of the metal cations to DB18C6 at the S_0 state, which decrease as the radius of the metal cation increases. The binding energies at the S_1 state were also estimated from the gas-phase binding energies at the S_0 state and the experimental transition energies to the origin bands of the S_1 state. It was found that the binding energies at the S_1 state decreased to 94.4−95.6% of those at the S_0 state, regardless of the identity of the metal cation bound to DB18C6. This was ascribed to the fact that the contribution of 2p orbitals of the six oxygen atoms to the electron density of an overall MO is reduced by almost the same amount for all M^+-DB18C6 upon excitation from HOMO to LUMO. The origin-band widths of K^+-, Rb^+-, and Cs^+-DB18C6 were observed to be narrower than those of Li^+- and Na^+-DB18C6, which was attributed to the decrease in the number of possible conformers of DB18C6 by complexing with K^+, Rb^+, and Cs^+.

This study manifests the versatility of the gas-phase spectroscopy of M^+-DB18C6 over the solution-phase one as a tool of confirming the formation of DB18C6 complex ions with metal cations, identifying the metal cations bound to DB18C6, and even estimating their relative binding energies.

Acknowledgment. This work was supported by the Korea Research Foundation Grant (KRF-2005-202-C00171).

Supporting Information Available: Vertical singlet excitation energies predicted by TD-DFT and the pictorial representations for HOMOs and LUMOs of M^+-DB18C6. This material is available free of charge via the Internet at http://pubs.acs.org.

References and Notes

(1) Pedersen, C. J. *J. Am. Chem. Soc.* **1967**, *89*, 7017.
(2) Pedersen, C. J. *Science* **1988**, *241*, 536.
(3) Izatt, R. M.; Bradshaw, J. S.; Nielsen, S. A.; Lamb, J. D.; Christensen, J. J.; Sen, D. *Chem. Rev.* **1985**, *85*, 271.
(4) Gokel, G. W.; Leevy, W. M.; Weber, M. E. *Chem. Rev.* **2004**, *104*, 2723.
(5) Horwitz, E. P.; Dietz, M. L.; Fisher, D. E. *Solvent Extr. Ion Exch.* **1991**, *9*, 1.
(6) Bradshaw, J. S.; Izatt, R. M. *Acc. Chem. Res.* **1997**, *30*, 338.
(7) Basilio, N.; Garcia-Rio, L.; Mejuto, J. C.; Perez-Lorenzo, M. *J. Org. Chem.* **2006**, *71*, 4280.
(8) Ly, T.; Julian, R. R. *J. Am. Soc. Mass Spectrom.* **2006**, *17*, 1209.
(9) Chu, I.-H.; Zhang, H.; Dearden, D. V. *J. Am. Chem. Soc.* **1993**, *115*, 5736.
(10) Anderson, J. D.; Paulsen, E. S.; Dearden, D. V. *Int. J. Mass Spectrom.* **2003**, *227*, 63.
(11) Maleknia, S.; Brodbelt, J. *J. Am. Chem. Soc.* **1992**, *114*, 4295.
(12) More, M. B.; Ray, D.; Armentrout, P. B. *J. Am. Chem. Soc.* **1999**, *121*, 417.
(13) Feller, D. *J. Phys. Chem. A* **1997**, *101*, 2723.
(14) Grootenhuis, P. D. J.; Kollman, P. A. *J. Am. Chem. Soc.* **1989**, *111*, 2152.
(15) Glendening, E. D.; Feller, D.; Thompson, M. A. *J. Am. Chem. Soc.* **1994**, *116*, 10657.
(16) Yamashita, M.; Fenn, J. B. *J. Phys. Chem.* **1984**, *88*, 4451.
(17) Kusaka, R.; Inokuchi, Y.; Ebata, T. *Phys. Chem. Chem. Phys.* **2007**, *9*, 4452.
(18) Bourson, J.; Pouget, J.; Valeur, B. *J. Phys. Chem.* **1993**, *97*, 4552.
(19) Wang, Z.; Chang, S. H.; Kang, T. J. *Spectrochim., Acta Part A* **2008**, *70*, 313.
(20) Araki, Y.; Chitta, R.; Sandanayaka, A. S. D.; Langenwalter, K.; Gadde, S.; Zandler, M. E.; Ito, O.; D'Souza, F. *J. Phys. Chem. C* **2008**, *112*, 2222.
(21) Ghiggino, K. P.; Hutchison, J. A.; Islan, D.-M. S.; Araki, Y.; Ito, O.; Langford, S. J.; Lau, V.-L.; Takezaki, M. *Photochem. Photobiol. Sci.* **2006**, *5*, 1150.
(22) Erk, C. *Ind. Eng. Chem. Res.* **2000**, *39*, 3582.
(23) Shizuka, H.; Takada, K.; Morita, T. *J. Phys. Chem.* **1980**, *84*, 994.
(24) Nakamura, M.; Takahashi, K.; Fujioka, T.; Kado, S.; Sakamoto, H.; Kimura, K. *J. Am. Soc. Mass Spectrom.* **2003**, *14*, 1110.
(25) Yoon, T. O.; Choi, C. M.; Kim, H. J.; Kim, N. J. *Bull. Korean Chem. Soc.* **2007**, *28*, 619.
(26) Guan, S.; Marshall, A. G. *Int. J. Mass Spectrom. Ion Processes* **1996**, *157/158*, 5.
(27) Doroshenko, V. M.; Cotter, R. J. *Rapid Commun. Mass Spectrom.* **1996**, *10*, 65.

(28) Frisch, M. J. ; Trucks, G. W.; Schlegel, H. B.; Scuseria, G. E.; Robb, M. A.; Cheeseman, J. R.; Montgomery, J. A., Jr.; Vreven, T.; Kudin, K. N.; Burant, J. C.; Millam, J. M.; Iyengar, S. S.; Tomasi, J.; Barone, V.; Mennucci, B.; Cossi, M.; Scalmani, G.; Rega, N.; Petersson, G. A.; Nakatsuji, H.; Hada, M.; Ehara, M.; Toyota, K.; Fukuda, R.; Hasegawa, J.; Ishida, M.; Nakajima, T.; Honda, Y.; Kitao, O.; Nakai, H.; Klene, M.; Li, X.; Knox, J. E.; Hratchian, H. P.; Cross, J. B.; Adamo, C.; Jaramillo, J.; Gomperts, R.; Stratmann, R. E.; Yazyev, O.; Austin, A. J.; Cammi, R.; Pomelli, C.; Ochterski, J. W.; Ayala, P. Y.; Morokuma, K.; Voth, G. A.; Salvador, P.; Dannenberg, J. J.; Zakrzewski, V. G.; Dapprich, S.; Daniels, A. D.; Strain, M. C.; Farkas, O.; Malick, D. K.; Rabuck, A. D.; Raghavachari, K.; Foresman, J. B.; Ortiz, J. V.; Cui, Q.; Baboul, A. G.; Clifford, S.; Cioslowski, J.; Stefanov, B. B.; Liu, G.; Liashenko, A.; Piskorz, P.; Komaromi, I.; Martin, R. L.; Fox, D. J.; Keith, T.; Al-Laham, M. A.; Peng, C. Y.; Nanayakkara, A.; Challacombe, M.; Gill, P. M. W.; Johnson, B.; Chen, W.; Wong, M. W.; Gonzalez, C.; Pople, J. A. *Gaussian 03*, rev. C.02; Gaussian, Inc.: Wallingford, CT, 2004.

(29) Ohashi, K.; Nishi, N. *J. Phys. Chem.* **1992**, *96*, 2931.

(30) Takasu, R.; Nishikawa, K.; Miura, N.; Sabu, A.; Hashimoto, K.; Schulz, C. P.; Hertel, I. V.; Fuke, K. *J. Phys. Chem. A* **2001**, *105*, 6602.

(31) Izatt, R. M.; Christensen, J. J. *Synthetic Multidentate Macrocyclic Compounds*; Academic: New York, 1978.

(32) Shannon, R. D. *Acta Crystallogr.* **1976**, *A32*, 751.

(33) Jia, Y. Q. *J. Solid State Chem.* **1991**, *95*, 184.

(34) Hirata, S.; Lee, T. J.; Head-Gordon, M. *J. Chem. Phys.* **1999**, *111*, 8904.

(35) Rinkevicius, Z.; Tunell, I.; Salek, P.; Vahtras, O.; Agren, H. *J. Chem. Phys.* **2003**, *119*, 34.

(36) Yokojima, S.; Matsuda, K.; Irie, M.; Murakami, A.; Kobayashi, T.; Nakamura, S. *J. Phys. Chem. A* **2006**, *110*, 8137.

(37) Fang, J.; Li, J. *J. Mol. Struct.* **2002**, *593*, 179.

JP903832W